Semiclassical description of multiphoton processes

Gerd van de Sand[1] and Jan M. Rost[2]
[1]*Theoretical Quantum Dynamics, Fakultät für Physik, Universität Freiburg, Hermann-Herder-Straβe 3, D-79104 Freiburg, Germany*
[2]*Max-Planck-Institute for the Physics of Complex Systems, Nöthnitzer Straβe 38, D-01187 Dresden, Germany*
(Received 31 January 2000; published 12 October 2000)

We analyze strong field atomic dynamics semiclassically, based on a full time-dependent description with the Hermann-Kluk propagator. From the properties of the exact classical trajectories, in particular the accumulation of action in time, the prominent features of above-threshold ionization and higher-harmonic generation are proven to be interference phenomena. They are reproduced quantitatively in the semiclassical approximation. Moreover, the behavior of the action of the classical trajectories supports the so called strong field approximation which has been devised and postulated for strong field dynamics.

PACS number(s): 32.80.Fb, 03.65.Sq, 42.65.Ky

I. INTRODUCTION

In the last two decades multiphoton processes have been studied intensively, experimentally as well as theoretically. The inherently time-dependent nature of an atomic or molecular excitation process induced by a short laser pulse renders a theoretical description problematic in two respects. First, a full quantum calculation in three dimensions requires a large computational effort. For this reason, quantum calculations have been restricted to one active electron in most cases [1,2]. Secondly, an intuitive understanding of an explicitly time-dependent process seems to be notoriously difficult, exemplified by pertinent discussions about stabilization in intense laser fields [3–5]. Many studies have been carried out to gain an intuitive understanding of the two most prominent strong field phenomena, namely, high-harmonic generation (HHG) and above-threshold ionization (ATI). In the well established early analytical formulation by Keldysh, Faisal, and Reiss the atomic potential is treated as a perturbation of the motion of the electron in a strong laser field [6].

This picture is still used in more recent models, where the classical dynamics of the electron in the laser field is explicitly considered, e.g., in Corkum's rescattering model, which can explain the cutoff observed in HHG for linearly polarized laser light in one spatial dimension [7]. The corresponding Hamiltonian reads [8]

$$H = H_0 + E_0 f(t) x \sin(\omega_0 t + \delta), \tag{1}$$

where $H_0 = \frac{1}{2}p^2 + V(x)$ is the atomic Hamiltonian, $f(t)$ is the time profile of the laser pulse with maximum amplitude E_0, and ω_0 is the laser frequency. The interaction of the electron with the atom is specified by the potential V.

Lewenstein *et al.* extended Corkum's rescattering idea to a quasiclassical model that contains one (relevant) bound state not influenced by the laser field on the one hand and electrons that experience only the laser field on the other hand [9]. This simple model, sometimes also called the ''simple man's model'' [10], well explains qualitatively the features of HHG. The same is also true for an alternative model, where the electron is bound by a zero-range potential [11]. However, the basic question if and to what extent these multiphoton processes can be understood semiclassically, i.e., by interference of classical trajectories alone, remains unanswered. It is astonishing that no direct semiclassical investigation of the Hamiltonian Eq. (1) has been performed while a number of classical as well as quantum calculations for Eq. (1) have been published. However, only recently has a semiclassical propagation method been formulated that can be implemented with reasonable numerical effort. This is very important for the seemingly simple Hamiltonian Eq. (1) whose classical dynamics is mixed and in some phase space regions highly chaotic, which requires efficient computation to achieve convergence. Equipped with these semiclassical tools we have studied multiphoton phenomena semiclassically in the framework of Eq. (1). In comparison to the exact quantum solution, we will work out those features of the intense field dynamics that can be understood in terms of interference of classical trajectories.

The plan of the paper is as follows. In Sec. II we provide the tools for the calculation of a semiclassical, time-dependent wave function. In Sec. III we discuss above-threshold ionization and work out the classical quantities that structure the relevant observables semiclassically. In Sec. IV we use this knowledge for the description of higher-harmonic generation. Section V concludes the paper with a comparison of HHG and ATI from a semiclassical perspective, and a short summary.

II. CALCULATION OF THE SEMICLASSICAL WAVE FUNCTION

A (multidimensional) wave function $\Psi_\beta(\mathbf{x},t)$ can be expressed as

$$\Psi(\mathbf{x},t) = \int_0^t d\mathbf{x}' K(\mathbf{x},\mathbf{x}',t)\Psi(\mathbf{x}'). \tag{2}$$

Here, $\Psi(\mathbf{x}')$ is the initial wave function at $t=0$ and $K(\mathbf{x},\mathbf{x}',t)$ denotes the propagator. We will not use the well-known semiclassical Van Vleck–Gutzwiller (VVG) propagator, which is inconvenient for several reasons. First, one has to deal with caustics, i.e., singularities of the propagator, and, secondly, it was originally formulated as a boundary value problem. For numerical applications the so called Herman-Kluk (HK) propagator is much better suited (and for analyti-

cal considerations not worse); this is a uniformized propagator in initial value representation [12,13], which reads in a $2n$-dimensional phase space

$$K^{HK}(\mathbf{x},\mathbf{x}',t)=\frac{1}{(2\pi\hbar)^n}\int\int d\mathbf{p}d\mathbf{q}C_{\mathbf{qp}}(t)e^{iS_{\mathbf{qp}}(t)/\hbar} \times g_\gamma(\mathbf{x};\mathbf{q}(t),\mathbf{p}(t))g_\gamma^*(\mathbf{x}';\mathbf{q},\mathbf{p}) \quad (3)$$

with

$$g_\gamma(\mathbf{x};\mathbf{q},\mathbf{p})=\left(\frac{\gamma}{\pi}\right)^{n/4}\exp\left(-\frac{\gamma}{2}(\mathbf{x}-\mathbf{q})^2+\frac{i}{\hbar}\mathbf{p}(\mathbf{x}-\mathbf{q})\right) \quad (4)$$

and

$$C_{\mathbf{qp}}(t)=\left|\frac{1}{2}\left(\mathbf{Q_q}+\mathbf{P_p}-i\hbar\gamma\mathbf{Q_p}-\frac{1}{i\hbar\gamma}\mathbf{P_q}\right)\right|^{1/2}. \quad (5)$$

Each phase space point $(\mathbf{q},\mathbf{p})$ in the integrand of Eq. (3) is the starting point of a classical trajectory with action $S_{\mathbf{qp}}(t)$. The terms $\mathbf{X_y}$ in the weight factor $C_{\mathbf{qp}}(t)$ are the four elements of the monodromy matrix, $\mathbf{X_y}=\partial\mathbf{x}_t/\partial\mathbf{y}$. The square root in Eq. (5) has to be calculated in such a manner that $C_{\mathbf{qp}}(t)$ is a continuous function of t. The integrand in Eq. (3) is—depending on the system—highly oscillatory. Although the formulation presented is in the full dimensional space and there are no major obstacles to carrying out the calculation, we have restricted ourselves for this explorative study to one spatial dimension [see Eq. (1)] since the numerical effort is considerable (for the one-dimensional case the number of trajectories necessary for numerical convergence can already reach 10^7). We note in passing that an integration by the stationary phase approximation over momentum and coordinate variables reduces the HK propagator to the VVG propagator [14].

In all calculations presented here we have used a Gaussian wave packet as initial wave function,

$$\Psi_\beta(x')=\left(\frac{\beta}{\pi}\right)^{1/4}\exp\left(\frac{\beta}{2}(x'-q_\beta)^2\right). \quad (6)$$

With this choice, the overlap

$$f_{\gamma\beta}(q,p)\equiv\int g_\gamma^*(x';q,p)\Psi_\beta(x')dx' \quad (7)$$

can be calculated analytically and Eq. (2) reads, together with Eq. (3),

$$\Psi_\beta^{HK}(x,t)=\left(\frac{4\gamma\beta}{\alpha^2}\right)^{1/4}\frac{1}{2\pi\hbar}\int\int dpdqe^{iS_{qp}(t)/\hbar}C_{qp}(t) \times g_\gamma(x;q(t),p(t))f_{\gamma\beta}(q,p) \quad (8)$$

with $\alpha=\gamma+\beta$. For all results presented here we have taken $\gamma=\beta$.

For comparison with our semiclassical calculations we determined the quantum-mechanical wave function using standard fast-Fourier-transform split-operator methods [15].

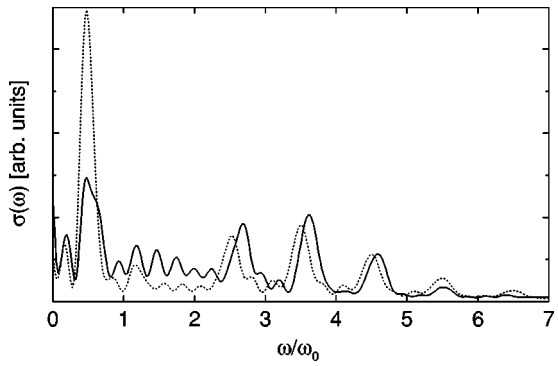

FIG. 1. Quantum-mechanical (dotted line) and semiclassical (solid line) ATI spectra for the Hamiltonian of Eq. (1) with $E_0=0.15$ a.u., $\omega_0=0.148$ a.u., and the soft-core potential Eq. (11).

III. ABOVE-THRESHOLD IONIZATION

We start from Eq. (1) with $\delta=0$ and use a rectangular pulse shape $f(t)$ which lasts for 4.25 optical cycles. This setting is very similar to the one used in [16].

The energy spectrum of the electrons can be expressed by the Fourier transform of the autocorrelation function after the pulse, i.e., for times $t>t_f$,

$$\sigma(\omega)=\mathrm{Re}\int_{t_f}^{\infty}e^{i\omega t}\langle\Psi(t)|\Psi_f\rangle dt, \quad (9)$$

where $\Psi_f=\Psi(t_f)$ is the wave function after the pulse and correspondingly

$$|\Psi(t)\rangle=e^{iH_0(t-t_f)/\hbar}|\Psi_f\rangle \quad (10)$$

is calculated by propagating Ψ_f for some time with the atomic Hamiltonian H_0 only after the laser has been switched off.

A. Quantum-mechanical and semiclassical spectra for ATI

We will present results for two types of potential to elucidate the dependence of the semiclassical approximation on the form of the potential.

1. Soft-core potential

First we apply the widely used softcore potential [16,17]

$$V(x)=-\frac{1}{\sqrt{x^2+a}} \quad (11)$$

with $a=1$ and with an ionization potential $I_p=0.670$ a.u. We have checked that the correlation function differs little if calculated with the exact ground state or with the ground state wave function approximated by the Gaussian of Eq. (6) where $\beta=0.431$ a.u. and $q_\beta=0$. However, the semiclassical calculation is considerably simplified with a Gaussian as initial state as can be seen from Eqs. (6)–(8). Therefore we use this initial state and obtain the propagated semiclassical wave function in the closed form, Eq. (8). In Fig. 1 the quantum and semiclassical results at a frequency $\omega_0=0.148$ a.u.

and a field strength $E_0=0.15$ a.u. are compared. The quantum-mechanical calculation (dotted line) shows a typical ATI spectrum. Intensity maxima with a separation in energy of $\hbar\omega_0$ are clearly visible. The first maximum has the highest intensity while the second maximum is suppressed.

The semiclassical result (solid line) is ambiguous: On the one hand there are clear ATI maxima with a separation of $\hbar\omega_0$. All peaks but the first one have roughly the correct magnitude. Again the second maximum is missing. On the other hand we see a constant shift (about 0.02 a.u.) of the spectrum toward higher energies. Therefore, a quantitative semiclassical description is impossible, at least with the present parameters and the soft-core potential. As it has turned out, in the time interval before ionization the bound electron wave packet evolves quite differently in the soft-core potential under quantum and semiclassical propagation. We will demonstrate that indeed the bound state dynamics is primarily responsible for the shift in the spectrum. This will be done by considering a different potential, which behaves almost harmonically for the lower bound states, implying a similar evolution of the wave packet under quantum and semiclassical propagation and thus eliminating this source of error.

2. Gaussian potential

A potential suitable for our purpose has been used to model the ''single bound state'' situation mentioned in the Introduction [18]. It is of Gaussian form,

$$V(x)=-V_0\exp(-\sigma x^2). \tag{12}$$

With our choice of parameters $V_0=0.6$ a.u. and $\sigma=0.025$ a.u., the potential contains six bound states and can be approximated, at least in the lower-energy part, by a harmonic potential for which semiclassical calculations are exact. Hence, the semiclassical ATI spectrum with this potential should be more accurate *if* the discrepancies in Fig. 1 are due to the potential and not to the laser interaction. The ground state wave function itself is again well approximated by the Gaussian Eq. (6) with $\beta=0.154$ a.u. and $q_\beta=0$. The laser has a frequency $\omega_0=0.09$ a.u., a field strength $E_0=0.049$ a.u., and a pulse duration of 4.25 cycles. The Keldysh parameter has the value 1.87.

We obtain a quantum-mechanical ATI spectrum (dotted line in Fig. 2) with six distinct maxima. The semiclassical spectrum (solid line) is not shifted; the locations of the maxima agree with quantum mechanics. Hence one can conclude that the soft-core potential is responsible for the shift. The height of the third maximum is clearly underestimated and the details of the spectrum are exaggerated by the semiclassical calculation. Apart from these deviations the agreement is good enough to use this type of calculation as a basis for a semiclassical understanding of ATI.

B. Semiclassical interpretation of the ATI spectrum

1. Classification and coherence of trajectories

With the chosen parameters most of the trajectories ionize during the pulse ($\sim$92%). We consider a trajectory as ionized if the energy of the atom

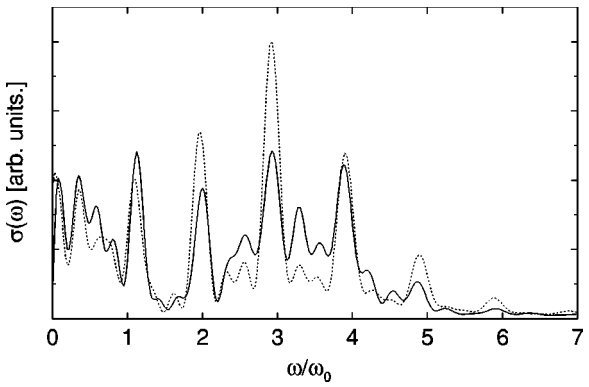

FIG. 2. Quantum-mechanical (dotted line) and semiclassical (solid line) ATI spectra for the Hamiltonian of Eq. (1) with $E_0=0.049$ a.u., $\omega_0=0.09$ a.u., and the Gaussian potential Eq. (12).

$$\varepsilon(t)=p(t)^2/2+V(q(t)) \tag{13}$$

becomes positive at some time t_n and remains positive, i.e., $\varepsilon(t)>0$ for $t>t_n$. Typically, the trajectories ionize around an extremum of the laser field. Tunneling cannot be very important, otherwise the agreement between quantum mechanics and semiclassics would be much worse.

An obvious criterion for the classification of the trajectories is the time interval of the laser cycle into which their individual ionization time t_n falls (see Fig. 3). Typically ionization of trajectory happens around $t_n=(2n-1)T/4$ when the force induced by the laser reaches a maximum. Hence, the ionized trajectories can be attached to time intervals $I_n=[(n-1)T/2,nT/2]$. In Fig. 3 we have plotted four trajectories from the intervals I_1 to I_4 that end up with an energy $E=0.36$ a.u. After ionization each trajectory shows a quiver motion around a mean momentum p_f [19]. One can distinguish two groups of intervals, namely, those with trajectories ionized with positive momentum p_f (the intervals I_{2k-1}) and those with trajectories with negative p_f (the intervals I_{2k}). These two groups contribute separately and incoherently to the energy spectrum, as one might expect since the electrons are easily distinguishable. One can see this directly from the

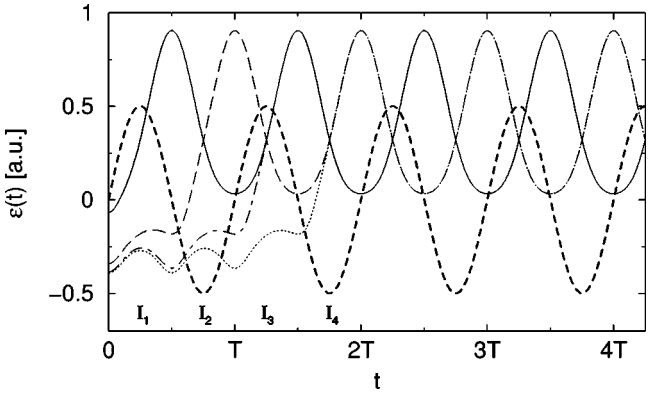

FIG. 3. Energy $\varepsilon(t)$ from Eq. (13) for some representative trajectories ionized in the intervals I_1 (solid line), I_2 (dashed line), I_3 (dash-dotted line), and I_4 (dotted line), respectively. For comparison, the laser field is plotted in arbitrary units (thick dashed line).

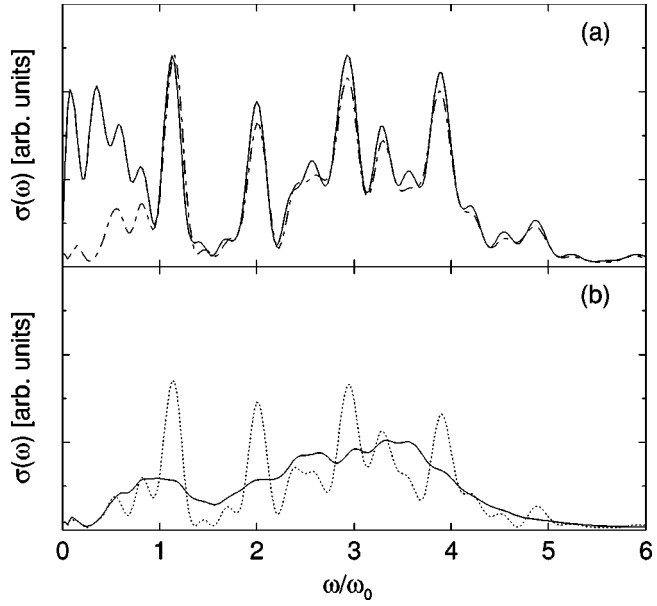

FIG. 4. (a) Semiclassical spectrum as an incoherent sum $\sigma_+(\omega)+\sigma_-(\omega)$ (dash-dotted line) compared with the full semiclassical spectrum (solid line). (b) Semiclassical spectrum $\sigma_+(\omega)$ constructed with trajectories from the intervals I_2, I_4, I_6, and I_8 (dotted) compared to the incoherent sum $\tilde{\sigma}_+$ of spectra that belong to the intervals I_2 to I_8 (solid line).

definition Eq. (9) of the electron energy spectrum. For relative high energies $\hbar\omega$ the (short-range) potential may be neglected in the Hamiltonian H_0 and we get

$$\begin{aligned}\sigma(\omega) &= \mathrm{Re}\int_{t_f}^{\infty} e^{i\omega t}\langle\Psi_f|e^{-iH_0(t-t_f)}|\Psi_f\rangle dt \\ &\approx \mathrm{Re}\int_{0}^{\infty} e^{i\omega t}\langle\Psi_f|e^{-ip^2t/2\hbar}|\Psi_f\rangle dt \\ &= \int_{-\infty}^{\infty}\delta(\omega-p^2/2\hbar)|\Psi_f(p)|^2 dp \\ &= [|\Psi_f(-\sqrt{2\hbar\omega})|^2+|\Psi_f(\sqrt{2\hbar\omega})|^2](\hbar/2\omega)^{1/2} \\ &\equiv \sigma_-(\omega)+\sigma_+(\omega). \end{aligned} \tag{14}$$

Hence, to this approximation, the ATI spectrum is indeed given by the incoherent sum of two terms belonging to different signs of the momenta of electrons ionized in different time intervals as described above.

Figure 4(a) shows that Eq. (14) is a good approximation. Only for small ω do the spectra not agree, where the kinetic energy is comparable with the (neglected) potential energy.

Quantum-mechanically, all contributions from trajectories that lead to the same momentum p_f of the electron are indistinguishable and must be summed coherently. To double check that the interference from different intervals I_n is responsible for the ATI peaks, we can artificially create a spectrum by an *incoherent* superposition $\tilde{\sigma}_+=\sigma_2+\sigma_4+\sigma_6+\sigma_8$ of contributions from trajectories ionized in the intervals I_{2j}.

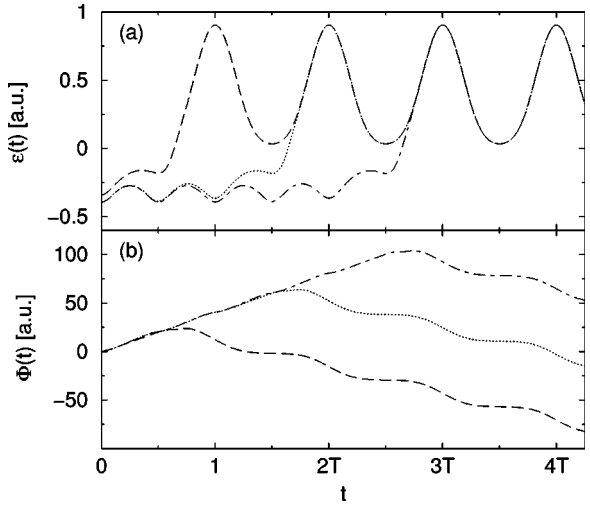

FIG. 5. (a) The atomic energy $\varepsilon=p^2/2+V(q)$ as a function of time for three trajectories from the intervals I_2 (dashed line), I_4 (dotted line), and I_6 (dash-dotted line). (b) The corresponding phases $\Phi(t)$.

This artificially incoherent sum [Fig. 4(b)] shows similarity neither with $\sigma_+(\omega)$ nor with any kind of ATI spectrum.

2. Classical signature of bound and continuum motion in the laser field

The great advantage of an *ab initio* semiclassical description lies in the possibility of making dynamical behavior transparent based on classical trajectories, particularly in the case of explicitly time-dependent problems where our intuition is not as well trained as in the case of conservative Hamiltonian systems. The classical quantities enter semiclassically mostly through the phase factor

$$\exp\{i[S_{qp}(t)-p(t)q(t)]/\hbar\}\equiv\exp[i\Phi/\hbar] \tag{15}$$

that each trajectory contributes to the wave function Eq. (8). Although the prefactor $C_{qp}(t)$ in Eq. (8) may be complex itself, the major contribution to the time dependence of the phase comes from the effective action Φ in the exponent of Eq. (15). Figure 5 shows the energy ε of the atom and the accumulated phase Φ. One can recognize a clear distinction between a quasifree oscillation in the laser field after the ionization and the quasibound motion in the potential. The latter is characterized by an almost constant averaged bound energy $\langle\varepsilon(t)\rangle$ [Fig. 5(a)] of the individual trajectory, giving rise to an averaged linear increase of the phase [Fig. 5(b)]. After ionization the phase decreases linearly with an oscillatory modulation superimposed by the laser field. The almost linear increase of Φ without strong modulation of the laser field during the bound motion of the electron is remarkable, particularly considering the laser induced modulations of the bound energy seen in Fig. 5(a). The averaged slope of the phase (positive for bound motion, negative for continuum motion) corresponds via $d\Phi/dt=-E$ to an averaged energy. The behavior can be understood by a closer inspection of the action

$$\Phi(t) \equiv S_{qp}(t) - p(t)q(t) = \int_0^t [2T - H - \dot{p}(\tau)q(\tau) - \dot{q}(\tau)p(\tau)]d\tau - qp. \tag{16}$$

Here, $T=p^2(t)/2$ refers to the kinetic energy and H to the entire Hamiltonian of Eq. (1), the overdot indicates a derivative with respect to time, and $q \equiv q(t=0)$. With the help of Hamilton's equations and a little algebra, Φ from Eq. (16) can be simplified to

$$\Phi(t) = -\int_0^t \left(\varepsilon(\tau) - q(\tau)\frac{dV}{dq} \right) d\tau \tag{17}$$

where ε is the atomic energy Eq. (13). With Eq. (17) we can quantitatively explain the slope of Φ in Fig. 5(b). For the low energies considered the potential Eq. (12) can be approximated harmonically,

$$V(q) \approx -V_0 + V_0 \sigma q^2. \tag{18}$$

Averaging Φ over some time then yields $\Phi(t) \approx V_0 t$ for *any* bound energy of a classical trajectory, since for an oscillator averaged kinetic and potential energy are equal. Indeed, the numerical value for the positive slope in Fig. 5(b) is 0.6 a.u. in agreement with the value for V_0.

For the ionized part of the trajectories we may assume that the potential vanishes. The corresponding solutions for electron momentum $p(t)$ follow directly from Hamilton's equation $\dot{p} = -E_0 \sin \omega_0 t$,

$$p(t) = \frac{E_0}{\omega_0}\cos(\omega_0 t) + p, \tag{19}$$

where p is the mean momentum. Without potential the phase from Eq. (17) reduces to $\Phi(t) = -\int p^2(\tau)/2 d\tau$ and we obtain with Eq. (19)

$$\Phi_c(t) = -\frac{U_p}{2\omega_0}\sin(2\omega_0 t) - \frac{E_0 p}{\omega_0^2}\sin\omega_0 t - (U_p + p^2/2)t \tag{20}$$

with the ponderomotive potential $U_p = E_0^2/4\omega_0^2$. We note in passing that Eq. (20) is identical to the time-dependent phase in the Volkov state (see the Appendix).

3. Semiclassical model for ATI

The clear distinction between classical bound and continuum motion in the laser field as demonstrated by Fig. 5 and illuminated in the last section allows one to derive easily the peak positions of the ATI spectrum. Moreover, this distinction also supports the so called strong field approximation (e.g., [9,20]) where electron dynamics in the laser field is modeled by one bound state and the continuum. While this is postulated in [9] as an approximation and justified *a posteriori* by the results, the corresponding approximation is suggested in the present context of a semiclassical analysis by the full classical dynamics, i.e., the behavior of the trajectories, as shown in Fig. 5. There, we saw that each classical bound motion leads to the characteristic linear increase of the phase. If the entire phase space corresponding to the initial (ground state) wave function is probed with many trajectories of different energy, the dominant contribution will appear at the bound state energy, which implies

$$\Phi_b(t) \approx I_p t, \tag{21}$$

where I_p is the ionization potential. The time for which a trajectory does not fall into one of the two classes, bound or continuum, is very short (Fig. 5). Hence, we can approximately compose the true phase $\Phi = \Phi_b + \Phi_c$. However, we do not know for an electron with mean momentum p when it was ionized. Hence, we have to sum over all trajectories with different ionization times τ but equal final momentum $p = p_f$, which leads to the propagated wave function

$$\Psi_f(t,p) \sim \int_{t_0}^t d\tau \exp\{i/\hbar[\Phi_b(\tau) + \Phi_c(t) - \Phi_c(\tau)]\} \sim \sum_{n,m} J_n\left(\frac{E_0 p}{\omega_0^2}\right) J_m\left(\frac{U_p}{2\omega_0}\right) \int_{t_0}^t d\tau e^{i\tau\Delta_{mn}/\hbar}, \tag{22}$$

where the phase Δ is given by

$$\Delta_{mn} = I_p + U_p + p^2/2 - (n+2m)\hbar\omega_0. \tag{23}$$

From Eq. (23) and Eq. (22) it follows that ATI peaks appear at integer multiples $n\hbar\omega_0$ of the laser frequency, when

$$\frac{p^2}{2} = n\hbar\omega_0 - I_p - U_p. \tag{24}$$

One can also see from Eq. (22) that the ATI maxima become sharper with each optical cycle that supplies ionizing trajectories. Of course, this effect is weakened by the spreading of the wave packet hidden in the prefactor of each trajectory contribution [see Eq. (8)] and not considered here.

Trajectories that are ionized during different laser cycles T accumulate a specific mean phase difference. The phase difference depends on the number k of laser cycles passed between the two ionization processes:

$$\Delta\Phi(p) = kT\left(I_p + \frac{p^2}{2} + U_p\right). \tag{25}$$

The trajectories interfere constructively if

$$\Delta\Phi(p) = 2\pi l \Rightarrow \frac{p^2}{2} = \frac{l}{k}\hbar\omega_0 - I_p - U_p. \tag{26}$$

If an energy spectrum is calculated exclusively with trajectories from two intervals separated by k cycles there should be additional maxima in the ATI spectrum with a separation $\hbar\omega_0/k$.

As a test for this semiclassical interpretation of the ATI mechanism we have calculated three spectra with trajectories where the mean time delay between ionizing events is given

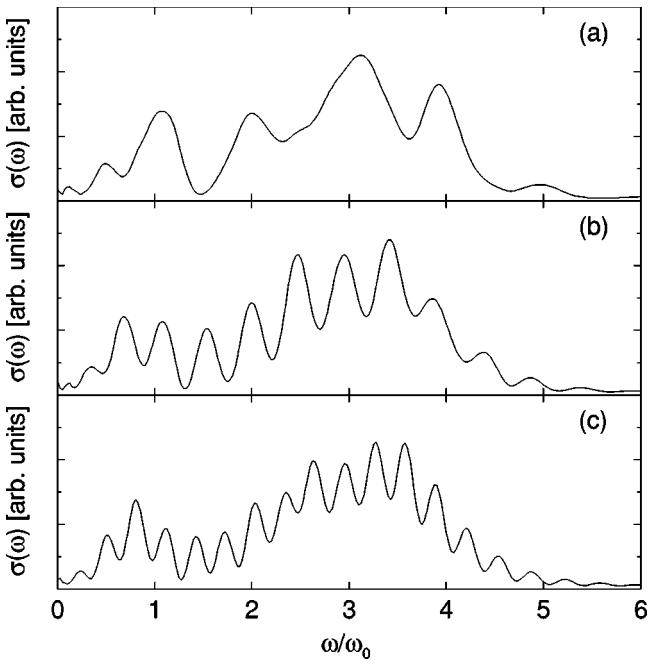

FIG. 6. Semiclassical spectra calculated with trajectories from the intervals I_2 and I_4 (a), I_2 and I_6 (b), and I_2 and I_8 (c).

by $\Delta t=T$, $\Delta t=2T$, and $\Delta t=3T$. For the spectrum Fig. 6(a) we have used exclusively trajectories from the intervals I_2 and I_4 ($\Delta t=T$). One can see broad maxima separated by $\hbar\omega_0$ in energy. Trajectories from the intervals I_2 and I_6 [see Fig. 6(b)] form a spectrum where the maxima are separated by $\hbar\omega_0/2$—as predicted for $\Delta t=2T$. In analogy, the separation for the ATI maxima in a spectrum with trajectories from the intervals I_2 and I_8 is given by $\hbar\omega_0/3$ [Fig. 6(c)]. The interference of trajectories ionized in many subsequent cycles suppresses the noninteger maxima and ultimately the well-known ATI results emerge. This can be understood from the way the number of realizations of a certain ratio l/k grows when the number k of cycles grows. Since the integer l is unlimited a certain integer i is realized by more combinations of l/n, $n\leqslant k$, than some rational fraction $1/j$. This discrepancy grows with increasing k and, as a consequence, fractional ATI peaks are suppressed with respect to integer peaks for a large number of laser cycles. On the other hand, if the field strength is high enough the atom is completely ionized during the first cycle. The opportunity for interference gets lost and we end up with an unstructured energy spectrum.

In an extreme semiclassical approximation we would have evaluated the integral in Eq. (22) by stationary phase. The condition

$$(d/d\tau)[\Phi_b(\tau)-\Phi_c(\tau)]\equiv I_p+p^2(\tau)/2=0 \qquad (27)$$

leads to complex ionization times t_n whose real part is periodic and allows for two ionizing events per laser cycle, close to the extrema of the laser amplitude. The derivation is simple but technical; therefore we do not carry it out explicitly here. However, it explains the observation that ionization occurs close to the extrema of the laser field and it also

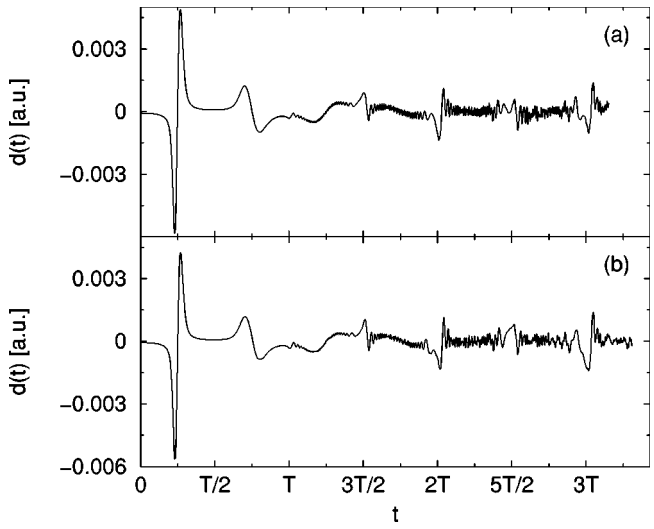

FIG. 7. Quantum (a) and semiclassical (b) dipole acceleration of higher harmonics according to Eq. (29).

makes contact with the tunneling process often referred to in the literature, since the complex time can be interpreted as tunneling at a complex ''transition'' energy.

Clearly, our semiclassical analysis as described here supports the picture that has been sketched in [21] interpreting a quantum calculation. The authors assume that wave packets are emitted every time the laser reaches an extremum. The interference of the different wave packets gives rise to the ATI peaks.

In the following we will discuss the process of higher-harmonic generation, which is closely related to ATI. In fact, the separation into a bound and continuum part of the electron description is constitutive for HHG as well; the prominent features, such as cutoff and peak locations, can be derived from the same phase properties Eq. (22) as for ATI. However, there is a characteristic difference: *how* these phases enter.

IV. HIGH-HARMONIC GENERATION

First, we briefly recapitulate the findings of [22], where we calculated the harmonic spectrum with the soft-core potential Eq. (11). With our choice of $a=2$ the ionization potential is given by $I_p=0.5$ a.u. The laser field has a strength $E_0=0.1$ a.u., a frequency $\omega_0=0.0378$ a.u., and a phase $\delta=\pi/2$. The initial wave packet with a width of $\beta=0.05$ a.u. is located at $q_\beta=E_0/\omega_0^2=70$ a.u. Note that the cutoff energy E_C in such a symmetric laser scattering experiment is given by

$$E_C=I_p+2U_p\,. \qquad (28)$$

From the dipole acceleration (see Fig. 7)

$$d(t)=-\left\langle \Psi(t)\left|\frac{dV(x)}{dx}\right|\Psi(t)\right\rangle, \qquad (29)$$

follows by Fourier transform

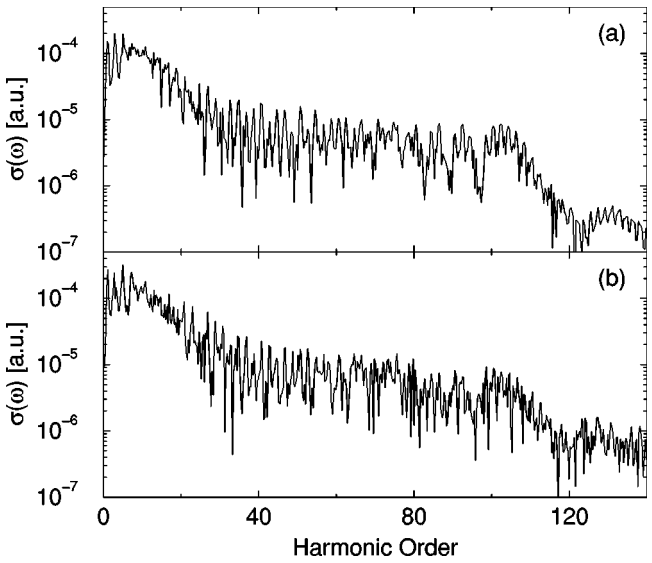

FIG. 8. Quantum (a) and semiclassical (b) spectrum of higher harmonics according to Eq. (30).

$$\sigma(\omega)=\int d(t)\exp(i\omega t)dt \tag{30}$$

the harmonic power spectrum (see Fig. 8).

Clearly, our semiclassical approach represents a good approximation. The dipole acceleration shows the characteristic feature that fast oscillations (which are responsible for the high harmonics in Fourier space) show up only after some time, here after $t=T$. This is the first time that trajectories are trapped. Trapping can occur only if (i) $t_n=nT/2$, (ii) the trajectories reach a turning point [i.e., $p(t_n)=0$], and (iii) at this time the electron is close to the nucleus [$q(t_n)\approx 0$]. The trapped trajectories constitute a partially bound state which can interfere with the main part of the wave packet (trajectories) still bouncing back and forward over the nucleus driven by the laser. The group of briefly bound (i.e., trapped or stranded) trajectories can be clearly identified, either by their small excursion in space [Fig. 9(a)] or by the positive slope of their action [Fig. 9(b)], as was the case for ATI (compare with Fig. 5). By artificially discarding the initial conditions in the semiclassical propagator that lead to trapped trajectories, one can convincingly demonstrate that the plateau in HHG generation is a simple interference effect [22]. Here, we are interested first in linking ATI to HHG by using the same separation in bound and continuum parts of the dynamics already worked out for ATI. Secondly, we want to go one step further and construct a wave function based on this principle.

Semiclassically, we have to look first at the phases of the observable. Therefore, we define a linear combination for the wave function from the respective phase factors for bound and continuum motion. Considering only terms in the exponent the harmonic spectrum Eq. (30) reads simply

$$\sigma(\omega)\sim\int dt\exp(i\omega t)\left|\exp[i\Phi_c(t)/\hbar]+c\exp[i\Phi_b(t)/\hbar]\right|^2, \tag{31}$$

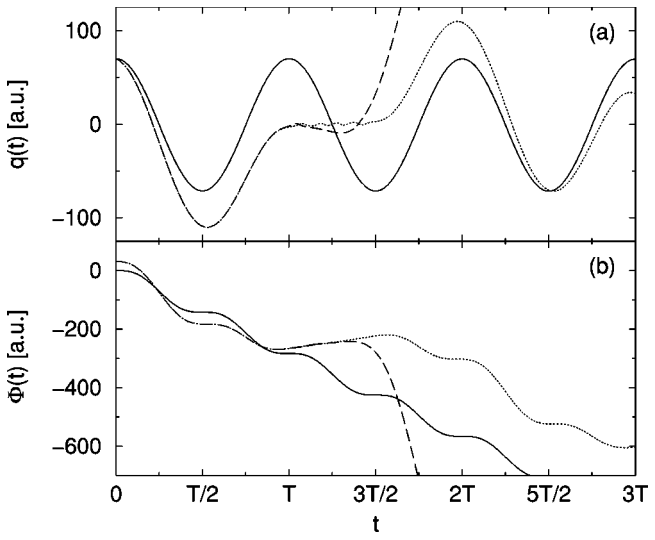

FIG. 9. Examples for direct (solid line), trapped (dotted line), and stranded (dashed line) trajectories; see text.

where $c\neq 0$ is a (so far) arbitrary constant. In principle, $c=c(t)$; however, its change in time is much slower than that of the optical oscillations of the phases $\Phi(t)$, hence we may approximate c by a constant. The bound and continuum phases Φ_b and Φ_c are defined in Eq. (21) and Eq. (20), respectively. For Φ_c we have $p=0$, since this is the dominant contribution from the center of the wave packet that was initially at rest. The result is shown in Fig. 10. Indeed, the plateau with the harmonics is generated; however, the initial exponential decrease is missing since we have neglected all prefactors of the semiclassical wave function that describe the dispersion of the wave packet.

Consequently, one can evaluate Eq. (31) in stationary phase approximation. The integrand of Eq. (31) becomes stationary if

$$\frac{d}{dt}\{\hbar\omega t\pm[\Phi_b(t)-\Phi_c(t)]\}=0, \tag{32}$$

which happens at

$$\hbar\omega=2U_p\sin^2(\omega t)+I_p. \tag{33}$$

From Eq. (33) we derive the cutoff law

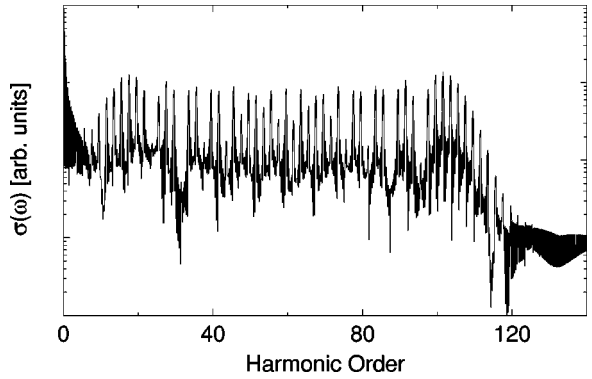

FIG. 10. Harmonic spectrum according to Eq. (31).

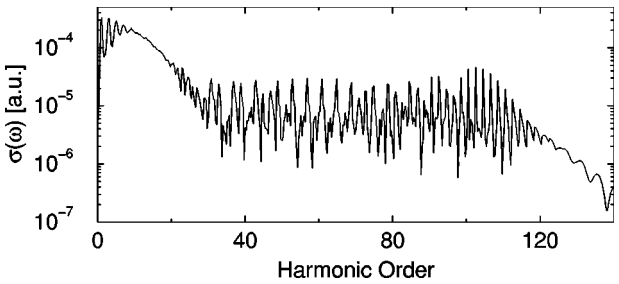

FIG. 11. Harmonic spectrum generated from the wave function Eq. (37) with $c=0.025$ and $\beta=0.05$ a.u.

$$\omega_{\max}=2U_p+I_p, \tag{34}$$

as expected for laser assisted electron ion scattering [22]. Using the same expansion into Bessel functions as in Eq. (22) we obtain for the spectrum Eq. (31)

$$\int dt\exp\left[\frac{i}{\hbar}\left((\hbar\omega-U_p-I_p)t+\frac{U_p}{2\omega_0}\sin(2\omega_0 t)\right)\right] = \sum_{k=-\infty}^{\infty}\int dt e^{it(\hbar\omega-U_p-I_p+2k\hbar\omega_0)/\hbar}J_k\left(\frac{U_p}{2\hbar\omega_0}\right). \tag{35}$$

Therefore, we see maxima in the harmonic spectrum for

$$\hbar\omega_k=U_p+I_p-2k\omega_0. \tag{36}$$

We can go one step further and construct a full time-dependent wave function from this semiclassical approximation, namely,

$$\Psi(x,t)=\Psi_\beta^{sc}(x,t)+c\Psi_0(x)\exp(itI_p/\hbar). \tag{37}$$

Here, $\Psi_0(x)\exp(iI_pt/\hbar)$ is the time-dependent ground state wave function (without the laser field) and $\Psi_\beta^{sc}(x,t)$ is a (semiclassical) *wave packet* in the laser field but without potential. Calculating the dipole acceleration and the resulting harmonic spectrum with this wave function leads to a remarkably good approximation of the true quantum spectrum (compare Fig. 8 with Fig. 11). The dispersion of the wave packet leads to a lower plateau compared to Fig. 10.

V. CONCLUSIONS

A. Semiclassical comparison between ATI and HHG

Clearly, the main structures, such as the plateau and cutoff (HHG), and the occurrence of peaks and their separation in energy (ATI and HHG), are properties of the difference of the classical time-dependent actions $\Phi_b(t)-\Phi_c(t)$ alone. However, the HHG power spectrum Eq. (30) is an integral over all the time for which the electron wave packet is exposed to the laser field. In contrast, the ATI spectrum is obtained in the long-time limit $t\to\infty$ after the laser has been switched off. This difference may explain why the HHG results tend to be better than the ATI results semiclassically: Any semiclassical approximation (which is not exact) become worse for large times.

A second point refers to the fact that the characteristic phase difference $\Phi_b(t)-\Phi_c(t)$ already appears in the wave function Eq. (22) for ATI, while for HHG it occurs only in the expectation value Eq. (29). However, this difference is artificial, since the expectation value, or, better, its Fourier transform the power spectrum, is not the observable of higher-harmonic radiation. The correct expression is the dipole-dipole correlation function R, which can be approximated as $R\propto|\sigma(\omega)|^2$ under single atom conditions or in the case of an ensemble of independent atoms that radiate [11,23]. Hence, in both ATI and HHG the peak structure already appears on the level of the quantum amplitude (or wave function) and is amplified in the true observable.

B. Summary

We have given a time-dependent fully semiclassical description of multiphoton processes. The prominent ATI and HHG features emerge naturally from properties of the classical trajectories whose contributions to the semiclassical wave function interfere semiclassically. Any effect of this semiclassical interference can be double checked by disregarding the phases. This leads (with the same trajectories) to a classical observable. As we have seen, to a good approximation the classical action for an individual trajectory can be composed of one part Φ_b for the time the electron is bound (disregarding the laser field) and another part Φ_c for the time the electron is in the continuum (disregarding the atomic potential). The relevant phase difference $\Phi_b-\Phi_c$ leads in both ATI and HHG to prominent harmonic structures in terms of the laser energy $\hbar\omega_0$. Finally, we have been able to construct a simple wave function for higher harmonics generated in laser assisted scattering. Its key element is an explicitly time-dependent wave packet of the electron under the influence of the laser field. Starting from an initial Gaussian distribution localized in space the wave packet disperses in time, providing the correct decrease of the intensity of the lower harmonics and in turn the correct height of the plateau.

ACKNOWLEDGMENT

Financial support from the DFG under the Gerhard Hess-Programm and the SFB 276 is gratefully acknowledged.

APPENDIX

We want to calculate the semiclassical wave function of a free particle in a laser field according to Eq. (8). A particle in a laser field $V_L(x,t)=E_0\sin(\omega t)$ moves with

$$p(t)=p+\frac{E_0}{\omega}\cos(\omega t)\equiv p+\tilde{p}(t), \tag{A1}$$

$$q(t)=q+pt+\frac{E_0}{\omega^2}\sin(\omega t)\equiv q+pt+\tilde{q}(t). \tag{A2}$$

The weight factor $C_{qp}(t)$ is given by

$$C_{qp}(t)=\left(1-\frac{i\hbar\gamma}{2}t\right)^{1/2}. \tag{A3}$$

For the phase factor $S_{qp}(t)-p(t)q(t)$ we get

$$S_{qp}(t)-p(t)q(t)=-\frac{U_p}{2\omega}\sin(2\omega t) - U_p t-\frac{p^2}{2}t-\tilde{q}(t)p-qp. \tag{A4}$$

Evaluating Eq. (8) with the stationary phase approximation, which is exact for quadratic potentials, leads to the condition that

$$f(q,p)=\frac{i}{\hbar}\left(xp(t)-\frac{p^2}{2}t-\tilde{q}(t)p-\frac{\gamma}{\alpha}qp-\frac{\beta}{\alpha}q_\beta p\right) - \frac{\gamma}{2}[x-q(t)]^2-\frac{\gamma\beta}{2\alpha}(q-q_\beta)^2-\frac{1}{2\hbar^2\alpha}p^2 \tag{A5}$$

must have an extremum. With

$$\frac{\partial f}{\partial q}=0=\gamma[x-q(t)]-\frac{\gamma\beta}{\alpha}(q-q_\beta)-\frac{i}{\hbar}\frac{\gamma}{\alpha}p, \tag{A6}$$

$$\frac{\partial f}{\partial p}=0=\gamma[x-q(t)]t-\frac{1}{\hbar^2\alpha}p + \frac{i}{\hbar}\left(x-pt-\tilde{q}(t)-\frac{\gamma}{\alpha}q-\frac{\beta}{\alpha}q_\beta\right), \tag{A7}$$

we find

$$q_s=\frac{x-\tilde{q}(t)+i\hbar\beta t q_\beta}{1+i\hbar\beta t}, \tag{A8}$$

$$p_s=\frac{i\hbar\beta}{1+i\hbar\beta t}[x-\tilde{q}(t)-q_\beta]. \tag{A9}$$

After some algebra we arrive at the stationary exponent

$$f(q_s,p_s)=\frac{i}{\hbar}x\tilde{p}(t)-\frac{\beta}{2(1+i\hbar\beta t)}[x-\tilde{q}(t)-q_\beta]^2 = \frac{i}{\hbar}x\tilde{p}(t)-\frac{i}{\hbar}\frac{\hbar^2\beta^2 t}{2\sigma(t)}[x-\tilde{q}(t)-q_\beta]^2 - \frac{\beta}{2\sigma(t)}[x-\tilde{q}(t)-q_\beta]^2, \tag{A10}$$

where $\sigma(t)$ is given by

$$\sigma(t)=1+\beta^2\hbar^2t^2. \tag{A11}$$

The determinant of the second derivatives of f still has to be calculated. With

$$\frac{\partial^2 f}{\partial q^2}=-\frac{\gamma^4+2\gamma\beta}{\alpha},\quad \frac{\partial^2 f}{\partial p^2}=-\frac{i}{\hbar}t-\gamma t^2-\frac{1}{\hbar^2\alpha},$$

$$\frac{\partial^2 f}{\partial q\partial p}=-\frac{i}{\hbar}\frac{\gamma}{\alpha}-\gamma t, \tag{A12}$$

we get

$$\det\begin{pmatrix}\frac{\partial^2 f}{\partial q^2} & \frac{\partial^2 f}{\partial q\partial p}\\ \frac{\partial^2 f}{\partial p\partial q} & \frac{\partial^2 f}{\partial p^2}\end{pmatrix}=\frac{2\gamma}{\hbar^2\alpha}[(1-i\gamma\hbar t/2)(1+i\beta\hbar t)]. \tag{A13}$$

The factor γ cancels, as it should, and we are left with

$$\Psi_\beta^{sc}(x,t)=\left(\frac{\beta}{\pi}\right)^{1/4}\sqrt{\frac{1}{1+i\hbar\beta t}} \times\exp\left[\frac{i}{\hbar}\left(\tilde{p}(t)x-\frac{U_p}{2\omega}\sin(2\omega t)-U_p t\right)\right] \times\exp\left(\frac{i}{\hbar}\frac{\hbar^2\beta^2}{2\sigma(t)}[x-\tilde{q}(t)-q_\beta]^2 t\right) \times\exp\left(-\frac{\beta}{2\sigma(t)}[x-\tilde{q}(t)-q_\beta]^2\right). \tag{A14}$$

This semiclassical time-dependent wave packet is quantum-mechanically exact and corresponds to a superposition of Volkov solutions according to a Gaussian distribution at time $t=0$ [24]. The fact that the semiclassical wave function is exact is a direct consequence of the Ehrenfest theorem, which implies that interactions $V\propto x^n$, $n=0,1,2$, have quantum-mechanically exact semiclassical solutions.

[1] K. C. Kulander, K. J. Schafer, and J. L. Krause, Adv. At., Mol., Opt. Phys., Suppl. 1, p. 247 (1992).
[2] M. Protopapas, C. H. Keitel, and P. L. Knight, Rep. Prog. Phys. **60**, 389 (1997).
[3] K. C. Kulander, K. J. Schafer, and J. L. Krause, Phys. Rev. Lett. **66**, 2601 (1991).
[4] B. Sundaram and R. V. Jensen, Phys. Rev. A **47**, 1415 (1993).
[5] M. Yu. Ivanov, O. V. Tikhonova, and M. V. Feodorov, Phys.

Rev. A **58**, R793 (1998); O. V. Tikhonova, E. A. Volkova, A. M. Popov, and M. V. Feodorov, *ibid.* **60**, R749 (1999).
[6] F. H. M. Faisal, J. Phys. B **6**, L89 (1973); H. R. Reiss, Phys. Rev. A **22**, 1786 (1980).
[7] P. B. Corkum, Phys. Rev. Lett. **71**, 1994 (1993).
[8] M. Protopapas, D. G. Lappas, C. H. Keitel, and P. L. Knight, Phys. Rev. A **53**, R2933 (1995).
[9] M. Lewenstein, P. Balcou, M. Y. Ivanov, A. L'Huiller, and P. B. Corkum, Phys. Rev. A **49**, 2117 (1994).
[10] W. Becker, A. Lohr, and M. Kleber, Quantum Semiclassic. Opt. **7**, 423 (1995).
[11] W. Becker, S. Long, and J. K. McIver, Phys. Rev. A **50**, 1540 (1994).
[12] M. F. Herman and E. Kluk, Chem. Phys. **91**, 27 (1984).
[13] K. G. Kay, J. Chem. Phys. **100**, 4377 (1994).
[14] F. Großmann, Comments At. Mol. Phys. **34**, 141 (1999).
[15] J. A. Fleck, J. R. Morris, and M. D. Feit, Appl. Phys. **10**, 129 (1976).
[16] J. Javanainen, J. H. Eberly, and Q. Su, Phys. Rev. A **38**, 3430 (1988).
[17] D. G. Lappas, A. Sanpera, J. B. Watson, K. Burnett, P. L. Knight, R. Grobe, and J. H. Eberly, J. Phys. B **29**, L619 (1996).
[18] C. Figueira de Morisson Faria, M. Dörr, and W. Sandner, Phys. Rev. A **55**, 3961 (1997).
[19] As already discussed in [16] it is therefore important that the calculations are stopped at times $t_m=(2m-1)T/4$ so that the ionized trajectories terminate at a time where they have their mean momentum.
[20] M. Lewenstein, K. C. Kulander, K. J. Schafer, and P. H. Bucksbaum, Phys. Rev. A **51**, 1495 (1995).
[21] D. G. Lappas and P. L. Knight, Comments At. Mol. Phys. **33**, 237 (1997).
[22] G. van de Sand and J. M. Rost, Phys. Rev. Lett. **83**, 524 (1999).
[23] B. Sundaram and P. W. Milonni, Phys. Rev. A **41**, 6571 (1990).
[24] S. Virito, K. T. Taylor, and J. S. Parker, J. Phys. B **32**, 3015 (1999).